



# Innovative Ground Improvement with Chemical Grouts: Potential and Limits of Partial Saturation with Polymers

Paul Pratter · Conrad Boley · Yashar Forouzandeh

Received: 30 March 2022 / Accepted: 8 September 2022  
© The Author(s) 2022

**Abstract** Nowadays, polymers are well-established in geotechnical applications, for example as grouting material for soil and rock stabilization, or as grouting material for anchorages. Concerning ground improvement, the polymers act as a binder that, if cured, holds the grains together by adhesive and cohesive forces. This special characteristic enables the use of less material and therefore saves costs but requires detailed knowledge of the material behavior to avoid application errors. The subject of this research work are two different polymers, which are used for partial saturation of the ground. For the investigation of the mechanical and hydraulic properties of the ground improvement, the geotechnical testing program on the composite material of polymers and gravel is extended by special tests, such as rheometer tests, for chemical grouts. If the polymers are used correctly, the composite material can achieve a load-bearing capacity comparable to that of concrete while the

material remaining permeable. This is highlighted by strength tests on the composite material. Finally, the numerical calculation of a track ballast stabilization, using PFC-FLAC3D coupling, demonstrates the potential of the polymers for practical application and that even difficult ground conditions can be handled with it.

**Keywords** Chemical grouts · Ground improvement · Distinct element method · Polymers

## 1 Introduction

Polymers are well-established in geotechnical applications, for example as grouting material for soil and rock stabilization and, in addition to the conventional cementitious grouts, are present in all kind of foundation engineering projects. The application possibilities of chemical grouts range from soil to rock improvement, whereby different aims can be pursued. Among these are most notably the reduction of permeability, the reduction of deformation or settlements and the increase of the load-bearing capacity. The selection of the chemical grout and the technically correct application of the chemical grout are crucial for the success of the ground improvement. In this scientific research work, the potential and limitations of innovative ground improvements with a material made of gravel and polymer are presented.

---

P. Pratter (✉) · C. Boley  
Institute for Soil Mechanics and Geotechnical Engineering,  
Bundeswehr University Munich, Werner-Heisenberg-Weg  
39, 85577 Neubiberg, Bavaria, Germany  
e-mail: paul.pratter@unibw.de

C. Boley  
e-mail: conrad.boleym@unibw.de

C. Boley · Y. Forouzandeh  
Boley Geotechnik GmbH, Auenstraße 100, 80469 Munich,  
Bavaria, Germany  
e-mail: y.forouzandeh@boleygeotechnik.de

Polymer and gravel form a so-called composite. Composites are combinations of materials differing in composition, where the individual constituents, in this case polymer and gravel, retain their separate identities. These separate constituents act together to give the necessary mechanical strength or stiffness to the composite part. Composite material is a material composed of two or more distinct phases (matrix phase and dispersed phase) and having bulk properties significantly different from those of any of the constituents (Jose et al. 2012). A special characteristic of the composite is partial saturation.

Thus, the composite can be distinguished from chemical grouts like acrylate or acrylamide and colloidal silica, whose use in non-cohesive soils primarily aims at a full saturation of the effective pore space and, consequently, at a reduction of the permeability, and respectively the sealing of the ground. The unconfined compressive strength (UCS) of these ground improvements tends to be secondary and is in the order of 0.8 MPa for a sand fully saturated with acrylate or acrylamide grouts (Boley et al. 2019; Chhun et al. 2019; Ozgurel and Vipulanandan 2005). Boley et al. (2019) determined the UCS-value of 0.8 MPa experimentally on grouted sand samples. Comparable values are determined in experimental laboratory tests by Chhun et al. (2019) on a grouted silty sand. For colloidal silica grouts the unconfined compressive strength (UCS) is about 0.3–0.5 MPa (Perhoff et al. 1999; Kutzner 1991; Ciardi et al. 2021). In particular, the review by Ciardi et al. (2021) on studies of colloidal silica grouts indicates an increase in load-bearing capacity with increasing curing time. The value range of about 0.3–0.5 MPa represents a curing time of 7 to 30 days, which is comparable to the samples of this research work. To stabilize the granular soil and increase the strength significantly, up to the order of magnitude of concrete, requires the use of high-strength resins (Spagnoli 2018), which are used, for example, in crack injection for rock stabilization (Forouzandeh et al. 2020).

In this context, the compressive strength is one of the most important properties of the cemented ground and is approximately proportional to the filling of the effective pore space with grout (Kutzner 1991). It is precisely this relationship of strength and saturation of soil stabilized with chemical grouts that the present research work focuses on. A composite of high-strength resins and gravel is investigated, which is

present, for example, in track ballast stabilization, or is itself used as a composite material for improvement in a low load-bearing ground. In addition to technical advantages, such as the adjustable load-bearing capacity and the controllable deformation behavior, as well as the always available drainage possibility, the partial saturation also results in greater economic opportunities and ecological potentials compared to conventional grouts. To benefit from the advantages and not risk serious technical errors, the use of polymers in geotechnical engineering requires a detailed understanding of the chemical properties and reaction processes. This regards in particular to the time-dependent viscoelastic behavior of the polymers, which is investigated using state-of-the-art methods, such as rheometer tests.

## 2 Ground Improvement with Polymers

There are different types of chemical grouts. In Spagnoli (2018), the chemical grouts are characterized in detail and classified into the following groups:

- Sodium silicate
- Colloidal silica
- Resin
- Polymers, like acrylate polymer or acrylamide grout

In this research work, two different synthetic resins are presented. The resins 01 and 02 can be characterized as bi-component resin grouts, which differ in terms of flow and deformation behavior as well as strength. Basically, the resins differ in their chemical composition, for example by a hardener. Therefore the properties of the resins are not adjusted by the mixing ratio or by additives. Both resins can be classified as thermosets. Thermosets are polymer networks where the junctions and stands are typically connected via covalent bonds, see Fig. 1. These materials are rigid, with a Young's moduli of about  $1E+09$  Pa, normally insoluble in all solvents and not processable once formed (Gu et al. 2020). Consequently the resins are water-resistant so that an application below the groundwater level is possible.

The resin "cements" the individual gravel grains and creates an effective bond between them, see

**Fig. 1** Thermosets are a class of static networks that have been covalently bonded, usually by heating to a temperature ( $T_f$ ) conducive to bond formation (curing) (Figure according to Webber and Tibbitt 2022)

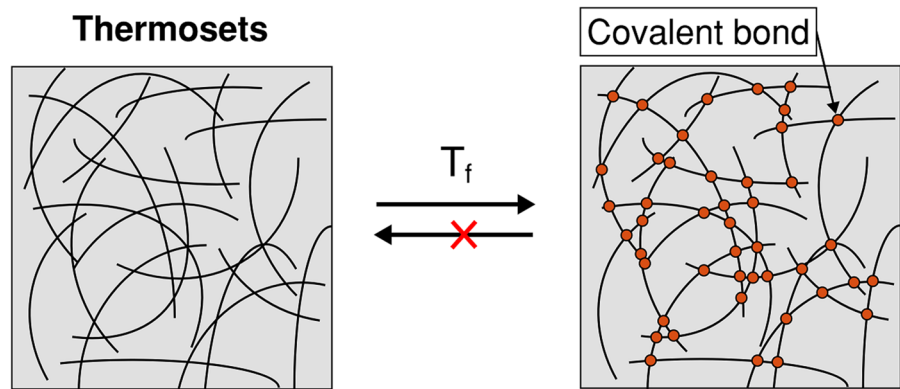


**Fig. 2** Microscopic analysis of the composite material: Defective and intact adhesive bond (a) and section through intact composite material, post-processed by image segmentation (b)

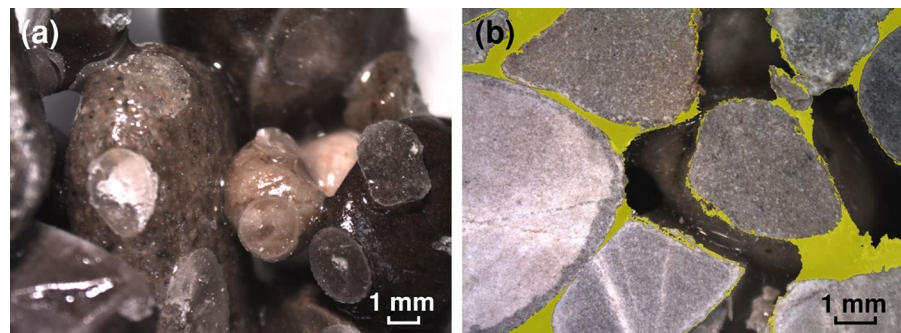


Fig. 2. For the formation of firm and permanent adhesive bonds, the surface of the material on the one hand and the internal strength of the adhesive on the other hand are crucial. Compared to the adhesive forces, which can be increased, for example, by cleaning the material surface, the strength and functionality of the adhesive connection is determined to a greater extent by the cohesive forces that develop inside the adhesive and depend on the polymer properties. The partial saturation of the gravel with resin is clearly visible from the microscopic analysis. In the sectional view in Fig. 2b, the resin was captured by image segmentation and highlighted in yellow. On the one hand, this shows very clearly that drainable porosity remains, so that flow processes are possible in the pore space, and on the other hand, resin menisci at the grain-to-grain contact characterize the intact adhesive bond. Defective, respectively detached, adhesive bonds are characterized by shell-like resin leavings with a central defect at the former grain-to-grain contact point, see Fig. 2a.

## 2.1 Rheological Properties of the Polymers

Basically, the chemical reaction of A and B component of the bi-component resin grouts starts immediately after mixing and leads to the formation of the polymer AB. The subsequent workability time or pot life characterizes the available time between mixing a grout and its application (Habenicht 2009). This concept applies to adhesives where two components are mixed shortly before use. Polymerization commences on mixing and cross-linking occurs in all cases. Both processes cause viscosity to increase, and this will begin to hinder the wetting of the adherends. A critical point, however, is the gel point, where the viscosity increases greatly due to the adhesive becoming completely cross-linked (Da Silva et al. 2011). The rheological properties and in particular these characteristic times are studied in detail in the rheometer. In this research work, oscillatory rheology tests were carried out. The characteristic pot life and gel time must be determined by rheological investigations because chemical grouts do not contain suspended

solid particles, so that injectability is a function of viscosity and not particle size (Karol 2003). The processability of chemical grouts can be categorized based on viscosity and divided into three ranges (Kutzner 1991), see Fig. 3:

- A: Ideal range
- B: Practicable range
- C: Acceptable range

In particular, the time-dependent flow behavior is of great importance for the use of the polymers in geotechnical application. The following aspects are relevant:

- Injectability of the resins
- Workability time of the polymer and resulting timetable for the ground improvement work with the composite material
- Time until the composite material is load-bearing and thus functional

For this purpose, oscillatory rheology tests were carried out on the resins. Both resins were mixed, deaerated and after 10 min installed between the plate/plate measuring system of the rheometer. The constant temperature of 20 °C was created using a Peltier temperature device. The workability time of the resins can be determined with the development of the dynamic viscosity, based on detailed research of the rheological behavior. In the rheometer, the resins were exposed to an oscillating shear load, so that only

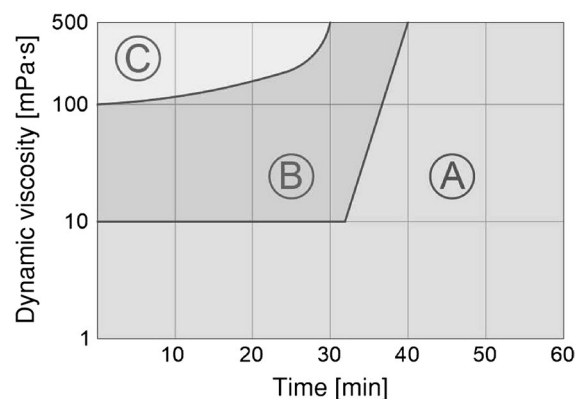


**Fig. 3** Ranges of processability of chemical grouts: **A** Ideal range, **B** Practicable range, **C** Acceptable range (Figure according to Kutzner 1991)

the real part of the complex viscosity  $\eta^*$  is relevant for determining the well-established material parameter dynamic viscosity  $\eta$ :

$$\eta^* = \frac{G''}{\omega} - i \frac{G'}{\omega} \quad (1)$$

$$\text{Re}(\eta^*) = \frac{G''}{\omega} = \eta \quad (2)$$

Where the viscoelastic material behavior is characterized by  $G'$  = storage modulus = elastic component,  $G''$  = loss modulus = viscous component (Mezger 2018) and  $\omega$  represents the angular frequency.

To evaluate the injectability and workability of the resins, Fig. 4 shows the time-dependent development of the dynamic viscosity of resin 01 and resin 02 at a temperature of 20 °C. For the evaluation of the measured values, the inflection tangents in the plateau region of the graphs were added. The pot life of the resins is about 22 min (resin 01) and 26 min (resin 02). These values do not consider the 10 min between the mixing of the A and B components and the start of the oscillatory rheology tests and are thus on the safe side with respect to the practical use. Looking at the order of magnitude of the dynamic viscosity, a large difference between the resins can be seen. Resin 01 has a viscosity of approximately 500 mPa·s and is thus acceptable or suitable for injections according to Fig. 3. This contrasts with resin 02, whose dynamic viscosity is approximately 1E+04 mPa·s and is consequently less suitable for injections.

Based on the rheological investigations, the time until the composite material is load bearing can be assumed. For this purpose, the gel point in Fig. 5 and the moment development in Fig. 6 are considered as parameters.

In a reactive adhesive, the time- and temperature-dependent sol–gel time or gel point represents the state at which the resin transitions from the increasingly higher viscosity to the solid range until the resin finally reaches its final strength (Habenicht 2009). Consequently, the gel point is the intersection of storage modulus  $G'$  and loss modulus  $G''$  (Mezger 2018) and is indicated in Fig. 5 for resin 01. The gel point of resin 01 is reached after approximately 230 min.

This evaluation method is only partially suitable for resin 02. Despite repeated measurements, the graph of the storage modulus  $G'$  shows a changeable

**Fig. 4** Time-dynamic viscosity curves of the resin 01 and resin 02 at 20 °C

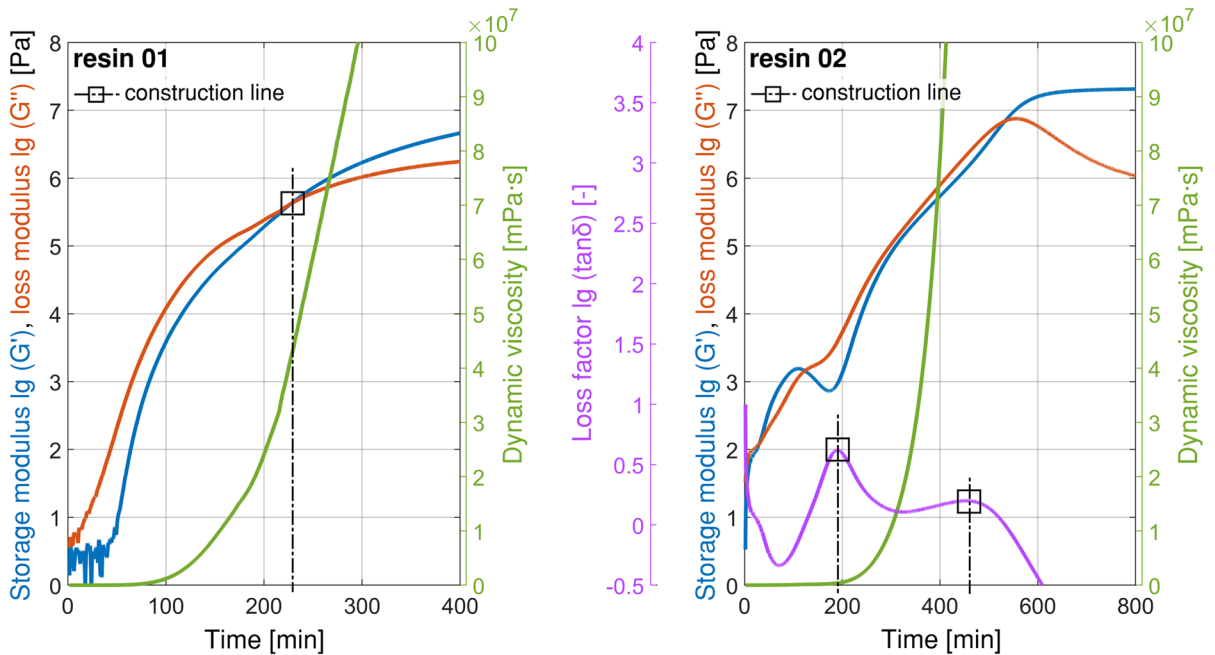
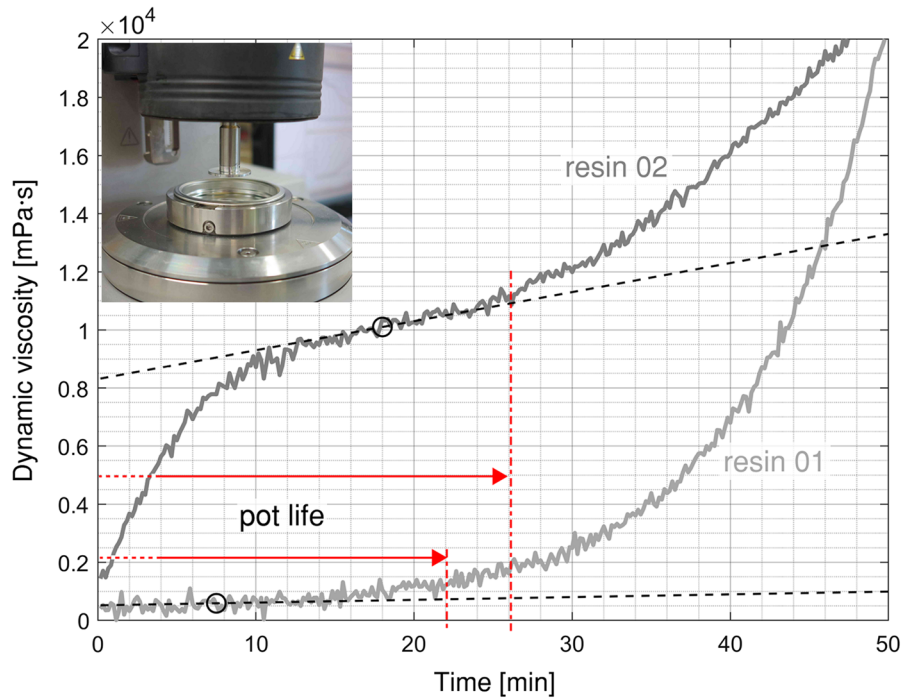


**Fig. 5** Storage and loss modulus of resin 01 (left) and resin 02 (right) at 20 °C

curvature behavior and intersects the graph of the loss modulus  $G''$  several times. Therefore, the graph of the loss factor is also mapped as an auxiliary

quantity. The loss factor  $\tan\delta$  represents the viscoelastic ratio and is defined according to Eq. 3. At the gel point, the maximum of the loss factor is located

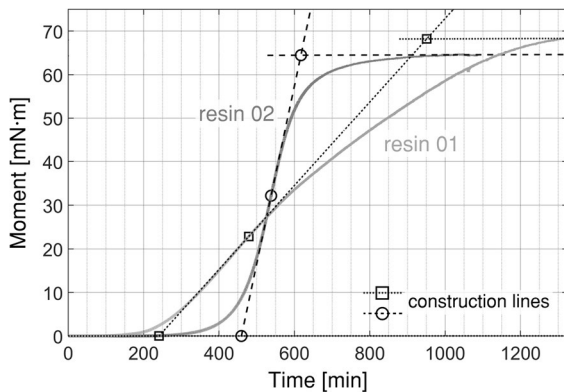


**Fig. 6** Time-moment curves of resin 01 and resin 02 at 20 °C

because there is a phase transition from the liquid sol state to the solid gel state (Mezger 2018).

$$\tan\delta = \frac{G''}{G'} \quad (3)$$

The loss modulus graph of resin 02 has reached a maximum at about 200 min and shows another maximum turning point at about 460 min. Considering the viscosity development between these points in time, the available data do not allow a clear determination of the gel point. The phase transition can only be localized to the interval from approx. 200 min to 475 min. This time interval is too imprecise for the determination of the time until the composite material is load bearing, therefore the time-dependent moment curves of resins 01 and 02 are additionally investigated. In general, the measured moment represents a physical measurand, which depends on the selected measuring system and can be converted into the rheological parameter shear stress (Mezger 2018).

To evaluate the moment development of resin 01 and resin 02 at 20 °C, the graphs are approximated by three tangential construction lines, see Fig. 6. The markers highlight the inflection point and the intersections with the horizontal construction lines. Basically, there are three different areas, which for the resin 01 at 20 °C lie in the following time periods:

- Fluid behavior ( $t < 230$  min): No bonding between resin and gravel.
- Gelation/curing ( $230 \text{ min} < t < 975$  min)

- Solid behavior ( $t > 975$  min): Firm adhesive bond between the gravel, which enables a force transmission. The composite material has an initial strength and can be subjected to mechanical loads.

The graphs in Fig. 6 show that resin 01 reaches the gel time earlier than resin 02, but then shows a flatter curve progression to solid behavior, with a maximum moment of approximately 68 mN·m, and thus cures more slowly. Consequently, resin 02 can be loaded earlier, since the initial strength is already reached after approximately 620 min and not after approximately 950 min, like resin 01.

Based on Fig. 5, the phase transition of resin 02 cannot be clearly determined and can only be localized to the time interval from approximately 200 min to 460 min. However, Fig. 6 shows that gelation/curing starts at approximately 460 min. This point in time marks the upper limit of the previously mentioned range and is evaluated as the gel point of the resin 02.

Generally, the initial strength of the composite material differs greatly from the final strength. The final strength of the composite material is about 4 to 5 times the initial strength and is reached after 7 days at 20 °C. After that, the strength of the composite material continues to increase, but not in the order of magnitude previously mentioned (Spagnoli 2018). For this reason, the tests on the mechanical behavior of the composite material are carried out on 7-day old samples.

## 2.2 Mechanical Behavior of the Composite Material

The mechanical behavior of the composite material was investigated through a large number of soil and rock mechanical laboratory tests. The test results are the basis for the numerical simulation and are evaluated in the present research work only regarding to the question of limit and risk in the case of partial saturation of the pore space. Partial saturation of the pore space with resin entails application risks if the rheological properties of the resin presented above are not considered during construction. For example, the wrong choice of chemical grout or exceeding the pot life can lead to inhomogeneous distribution of the resin in the composite material. The following comparison of the UCS of composite material with

homogeneous and inhomogeneous resin distribution clearly shows these differences.

The uniaxial compressive strength of the composite materials made of resin 01, 02 and gravel was investigated for a low mass fraction of resin and for a mass fraction of resin that was about three times higher. The samples with a high mass fraction of grout were prepared both homogeneously and inhomogeneously, to investigate the effects of an application error. Therefore, the inhomogeneous specimens were stored upright so that the flowable resins flowed into the lower third of the cylindrical specimen during curing and almost saturated it there.

Basically, cylindrical specimen with a height of approximately 100 mm and a diameter of approximately 50 mm were investigated. Due to the high strength of the composite material, the specimens were tested using the test technique for rock and subjected to a strain-controlled load of 0.1 mm/min. The uniaxial compressive tests were performed on 7-day old samples and at least five tests were carried out for each composite material. The test results are compared in Fig. 7.

Regarding to the reduction of the uniaxial compressive strength (UCS) due to an inhomogeneous distribution of the grout, resin 01 with approximately 9% deviates strongly from resin 02 with approximately 63%. The reason for this is the earlier increase in dynamic viscosity of resin 01 compared to resin

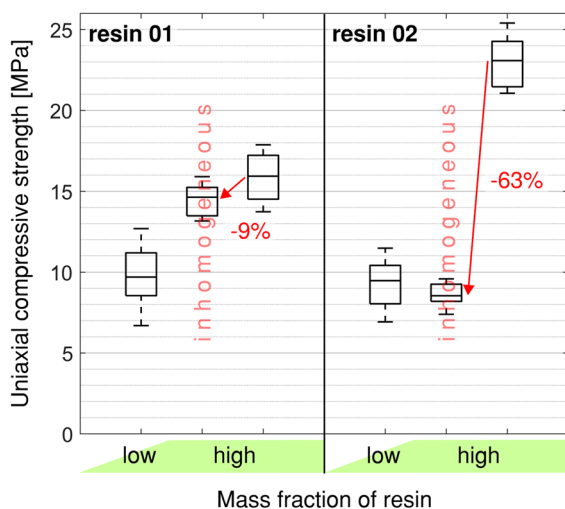


**Fig. 7** Uniaxial compressive strength of in-/homogeneous composites with resin 01, 02

02, see Fig. 5. Therefore, resin 01 in the upright specimen does not flow into the lower region of the specimen with the same mass fraction as resin 02, following gravity. This means that resin 01 is fundamentally less susceptible to errors regarding its practical use in construction. Furthermore, Fig. 7 clearly shows the potential, but also the risk, of partial saturation with resin 02. In the correct application, a UCS of about 9.5 MPa can be achieved even with a low mass fraction of resin 02. A high mass fraction even leads to a UCS of about 23.0 MPa, whereby the composite material still has a high permeability. If application errors occur, the UCS drops to values in the order of magnitude of the low mass fraction of resin 02, despite the high mass fraction of resin 02. At this point, not only a technical risk arises regarding the load-bearing capacity of the ground improvement and the characteristic values that were used in the planning of the ground improvement. There are also considerable monetary and ecological disadvantages. This is because one-third of the applied amount of resin 02 would have been sufficient to achieve a UCS of about 8.5 MPa.

### 3 Numerical Simulation

The numerical simulation shows the application potential of the innovative composite material based on the practical example of a track ballast stabilization. For this purpose, a coupled model of the three-dimensional discontinuum program “Particle Flow Code 3D” (PFC3D, Itasca Consulting Group, Inc.) and the explicit finite volume formulation “Fast Lagrangian Analysis of Continua in 3 Dimensions” (FLAC3D, Itasca Consulting Group, Inc.) is used. The track ballast is modeled using PFC3D and the underlying bedrock is modeled using FLAC3D. Before the comparative calculations can be performed, the track ballast, respectively the composite material, must be modeled in detail with PFC3D. The following steps are necessary:

1. Selection of a suitable contact model and material genesis
2. Calibration of the material, based on the laboratory tests
3. Finally, calculation of a track ballast stabilization by means of PFC-FLAC3D coupling

### 3.1 Numerical Model of the Composite Material

PFC3D is based on the distinct-element method. The interaction of the particles is treated as a dynamic process with states of equilibrium developing whenever the internal forces balance. The contact forces and displacements of a stressed assembly of particles are found by tracing the movements of the individual particles. Movements result from the propagation through the particle system of disturbances caused by wall and particle motion, externally applied forces, and body forces (Potyondy and Cundall 2004). Accordingly, it is important to select an appropriate contact model. Following the investigations of Itasca Consulting Group Inc (2021) and Holt et al. (2005) for rigid grains grouted with resins, a linear parallel bonded model was selected for the composite material. The linear parallel bond model provides the behavior of two interfaces. An infinitesimal, linear elastic (no-tension) and frictional interface that

carries a force and a finite-size, linear elastic and bonded interface that carries a force and moment, see Fig. 8. The second interface carries load only when it is bonded. Bonds are installed during material genesis at the grain-grain contacts with a gap less than or equal to the installation gap (Itasca Consulting Group Inc 2021). The installation gap was chosen according to Holt et al. (2005) and verified using the bond coordination number. The bond coordination number indicates the average number of intact bonds per grain. The grain size distribution of the uniform and round gravel of the laboratory samples was reproduced accordingly in PFC3D with balls and the porosity of the composite material was considered, see Table 1.

The microanalysis in Fig. 9 shows grouted glass bead and, in direct comparison, a section from the numerical model of the composite material. The parallels between the pictures are obvious. Furthermore, the partial saturation of the composite material. In the numerical model, between the dark gray and the light

**Fig. 8** Behavior and rheological components of the linear parallel bond model with inactive dashpots (Figure according to Itasca Consulting Group Inc (2021))

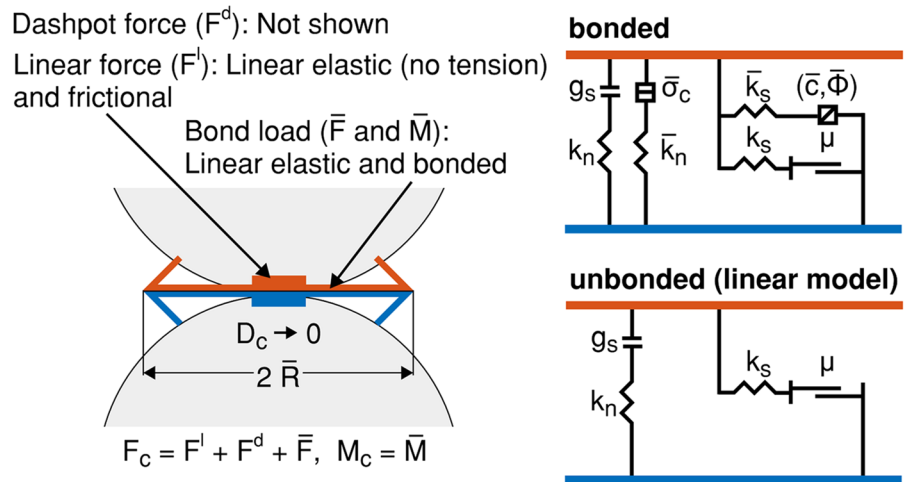
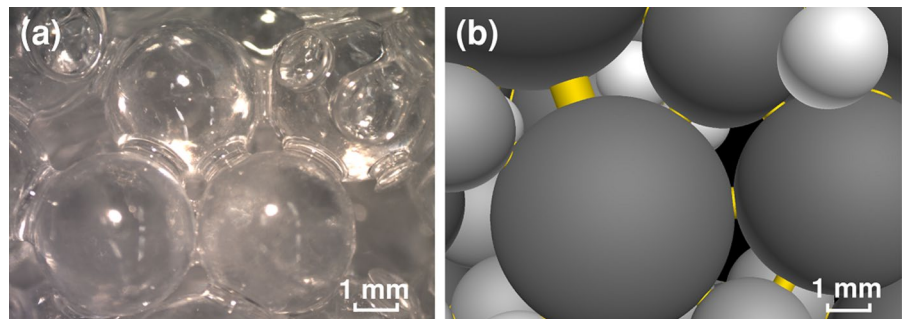


**Fig. 9** Grouted glass bead (a) and parallel-bonded particles in PFC3D (b)





gray ball, the installation gap was exceeded, and no yellow marked bond was formed, see Fig. 9.

### 3.2 Calibration and Verification of the Numerical Model

The calibration was performed according to recommendations of Potyondy (2018) and the sketch to illustrate the calibration of the micro-parameters presented in Zhao et al. (2021). Basically, the calibration is based on the macro-parameters determined by the physical experiments, for example UCS, Poisson’s ratio, Young’s modulus, and tensile strength. According to the difference between the macro-parameters obtained from the physical experiments and the numerical simulation, the micro-parameters are calibrated until the macro-parameters obtained from the numerical simulation are sufficiently closed to those from physical experiments, according to a trial-and-error method (Potyondy and Cundall 2004; Ajamzadeh et al. 2018).

Based on the results of the laboratory tests, the UCS, the Young’s modulus and peak strength of the composite material (PFC3D) are measured. The modulus is comparable with the target modulus, see Fig. 10. In addition, tensile tests were performed and the tensile strength ( $\sigma_t$ ) of the composite material

(PFC3D) adjusted to obtain target tensile strength. The calibrated composite material was verified using a series of triaxial tests with increasing confinements of 0.8 MPa, 1.6 MPa, 3.2 MPa to obtain the strength envelope. Figure 10 (right) confirms that strength should increase and the response should become less brittle with increasing confinement (Potyondy 2018). The micro-mechanical parameters of the calibrated composite material are excerpted in Table 1.

### 3.3 Numerical Simulation of a Track Ballast Stabilization

The numerical simulation is based on an already executed railway project, in which a tunnel in hard rock (gneiss) was reconstructed. To maintain two supply channels below the track ballast, a working space had to be created by removing the adjacent areas of the track ballast and sloping them steeply, see Fig. 11. Train traffic should still be possible, so the slope of the track ballast had to be stabilized. In the calculations, the high-performance resin O2 is used for this purpose because, in contrast to resin O1, it can be loaded earlier, see Fig. 6, and, if applied correctly, a higher load-bearing capacity can be achieved, see Fig. 7.

**Fig. 10** Results of the numerical simulation (orange/red) and physical experiments (grey): Unconfined (left) and triaxial compression tests (right)

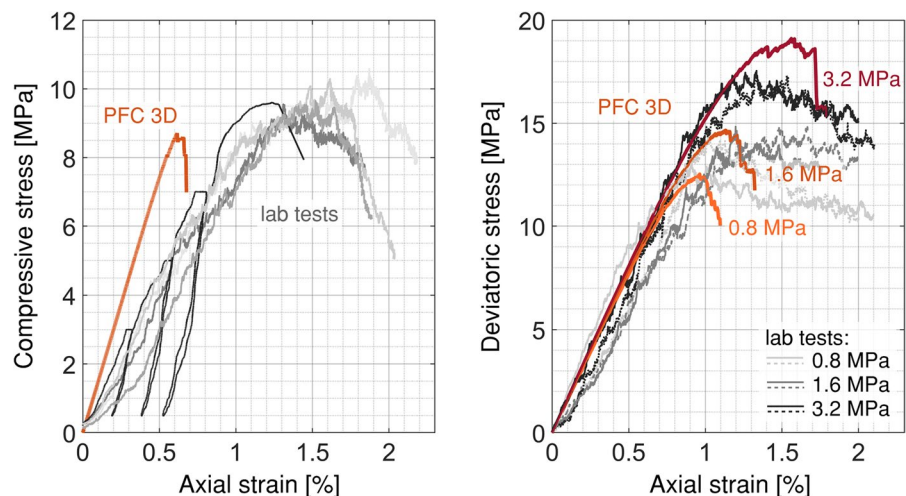


**Table 1** Micro-mechanical parameters of the composite material

$\rho$ ( $g/cm^3$ )	n	$D_{50}$ (mm)	$\bar{E}_c$ (GPa)	$\bar{k}_n/\bar{k}_s$	$\lambda$	$\sigma_t$ (MPa)	c (MPa)	$\phi$ ( $^\circ$ )
1.8	0.33	5.8	1.8	5	1	5.2	8.8	29.0

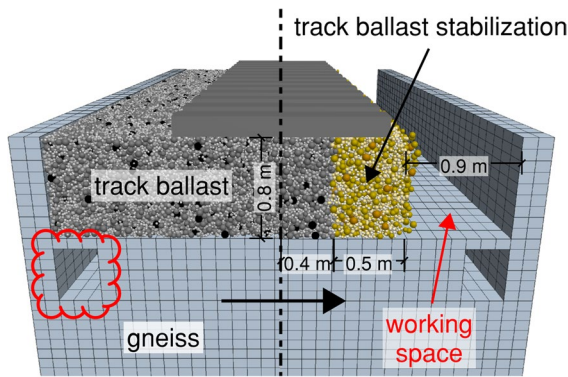


**Fig. 11** Numerical model before (left) and after (right) track ballast stabilization

The aim of the numerical simulation is to demonstrate a geotechnical application for the innovative composite material and to visualize the deformation and the load-bearing behavior. For this reason, static loads are modeled in the numerical calculation instead of dynamic loads. Axle loads of 100 kN were applied at a distance of 2.4 m and distributed evenly on two railway sleepers. The composite material was modeled using the micro-mechanical parameters presented in Table 1 and the grain size was scaled to that of the track ballast using the scaling factor 4. In principle, the track ballast is simulated using the distinct element method PFC3D.

The distinction between stabilized track ballast (Table 1) and track ballast without grout (Table 2) is made in PFC3D by grouping the individual particles. For the grain-grain contacts of the track ballast, which lies between the stabilized track ballast according to Fig. 11, only the linear model of Fig. 8 is valid. To represent the interaction between track ballast and gneiss, a coupled model of PFC3D and FLAC3D is used, so that the deformations, respectively stresses, in the gneiss can be determined and visualized. Table 2 also contains the geotechnical parameters for the gneiss, as well as corresponding values for the

selected failure criterion according to Hoek–Brown (Hoek 2007).

#### 4 Results of the Numerical Simulation and Discussion

Figure 12 shows the calculation results of the numerical simulation and particularly the potential of the innovative ground improvement based on a partial saturation with polymers. The displacement, stress and bond state plots provide the following information on the deformation and load-bearing behavior of the stabilized track ballast.

The track ballast grouted with resin 02 stabilizes the track ballast in between, thereby measurable deformations occur mainly in the track ballast and are significantly below 1 mm. In the stabilized track ballast, the deformations are almost constant over the entire cross-section, while in the track ballast without grout, deformations are primarily present in the upper half of the cross-section towards the railway sleeper. Consequently, the deformations in the gneiss and thus also in the supply channels are very small and negligible, see displacement plot in Fig. 12.

The loads of 50 kN per railway sleeper are transferred into the gneiss by the composite material, as with a rigid ground improvement. This can also be clearly seen from the fact that the track ballast without grout is no longer involved in load transfer into the gneiss, see stress plot in Fig. 12. Moreover, this result is consistent with the load transfer mechanism for rigid ground improvements described by Han (2014).

Stress peaks occur in the transition area between grouted and not grouted track ballast and are colored red in the stress plot in Fig. 12. It is precisely at these highly stressed areas that the bonds of the stabilized ballast track fail in isolated cases, see number 1 (red) in bond state plot in Fig. 12. In general, the stabilized track ballast (composite material) remains bonded and thus intact. Unbonded areas, number 0 in the

**Table 2** Micro-mechanical parameters for track ballast in general and gneiss according to Hoek (2007)

Track ballast			Gneiss							
$E_c$ (GPa)	$k_n/k_s$	$\mu$	$\rho$ (g/cm <sup>3</sup> )	E (GPa)	$\nu$	$\sigma_{ci}$ (MPa)	$m_b$	a	s	
0.1	1.5	0.4	2.7	20	0.24	170	28	0.5	1.25	

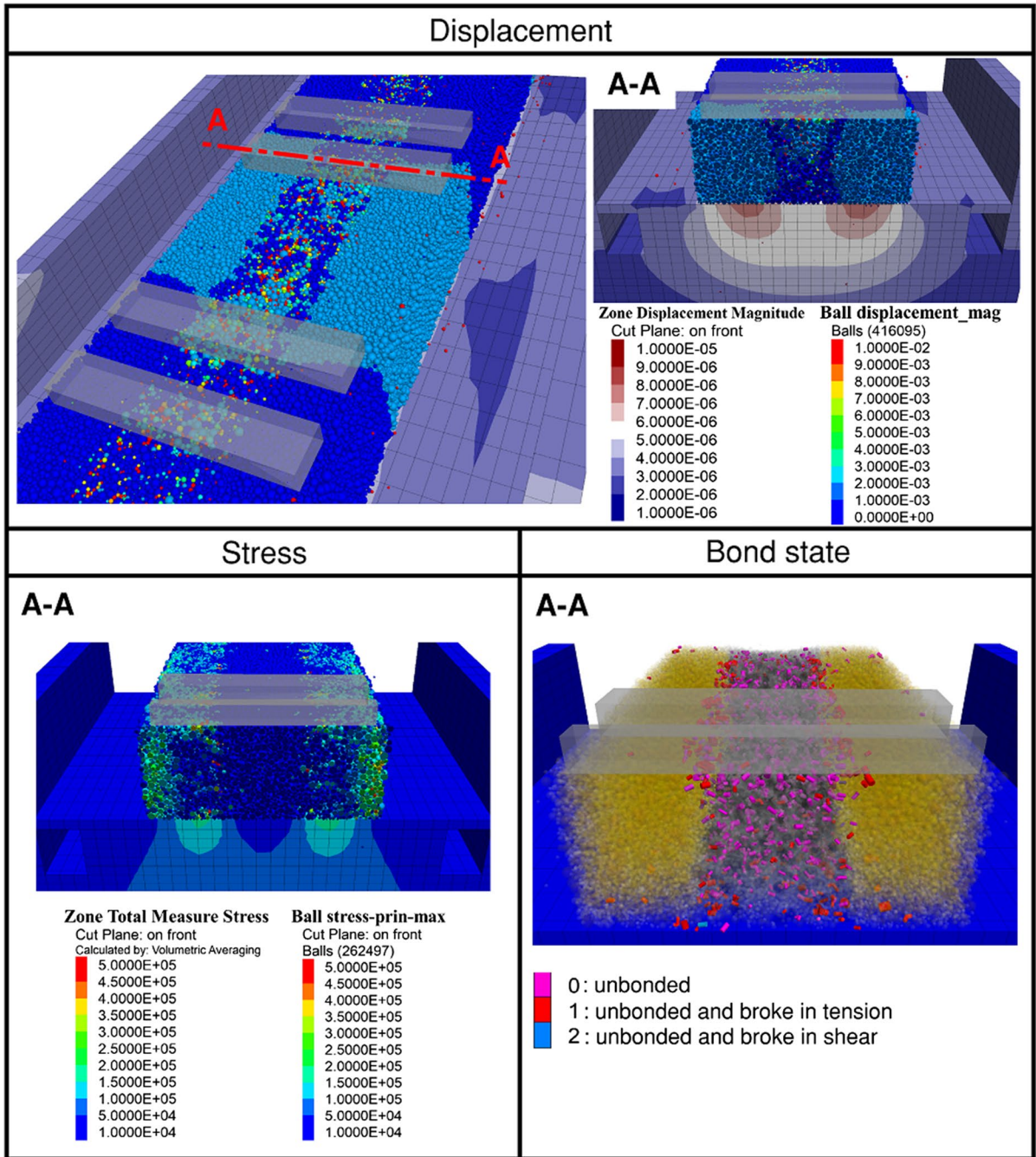


**Fig. 12** Results of the numerical simulation with PFC-FLAC3D coupling

bond state plot, occur exclusively in the not grouted track ballast.

Consequently, the practical example shows that the stabilized track ballast, respectively the

composite material in the present research work, created a working space for the maintenance of the supply ducts and at the same time ensured that train traffic is still possible.

## 5 Conclusions

Based on the results of the experimental research work it is obvious that the choice of the resin and the technically correct execution of the ground improvement have a significant influence on the construction. That must be considered when using polymer grouting technology in geotechnical engineering. The numerical calculations with the PFC-FLAC3D coupling have shown the potential of the innovative ground improvement for practical use in construction. Essentially, the findings of the present research work can be summarized as follows:

- Based on the microscopic analysis and the sectional view, post-processed by image segmentation, the partial saturation of the gravel with resin is clearly visible.
- The rheological properties of resins 01 and 02 differ significantly. While resin 01 has a comparatively low viscosity of 500 mPa·s and is in an acceptable range for injections, resin 02 has a viscosity of 1E+04 mPa·s and thus tends to be less suitable.
- The gel point of resin 01 could be clearly determined after 230 min with the oscillatory rheology tests, based on the intersection of storage and loss modulus. For resin 02, the time-moment curves also had to be evaluated. The gel point of resin 02 is at approximately 460 min.
- Although, resin 01 reaches the gel point before resin 02, resin 02 has initial strength after 10 h and can be subjected to mechanical loads, while resin 01 can be loaded only after approximately 16 h.
- Based on the UCS of homogeneous and inhomogeneous composite materials, it was shown that application errors, especially with resin 02, result in a technical risk regarding the load-bearing capacity of the ground improvement. In addition, there are also considerable monetary and ecological disadvantages. This is because one-third of the applied amount of resin 02 would have been sufficient to achieve a UCS of about 8.5 MPa.
- In the numerical simulations with PFC3D, the linear parallel bonded model proved to be suitable for simulating the composite material with resin 02.
- Basically, the practical example shows the strengths of the PFC-FLAC3D coupling. The

interactions in the track ballast and of the track ballast with the gneiss can be simulated in detail.

- The composite material stabilizes the not grouted track ballast and transfers the loads into the gneiss, as with a rigid ground improvement. In general, the stabilized track ballast (composite material) remains bonded and thus intact.

**Acknowledgements** We are grateful to Keller Grundbau GmbH and TPH Bausysteme GmbH for the financial support of this research.

**Funding** Open Access funding enabled and organized by Projekt DEAL. The authors have not disclosed any funding.

**Data Availability** Enquiries about data availability should be directed to the authors.

### Declarations

**Conflicts of Interest** The authors declare that they have no conflicts of interest.

**Open Access** This article is licensed under a Creative Commons Attribution 4.0 International License, which permits use, sharing, adaptation, distribution and reproduction in any medium or format, as long as you give appropriate credit to the original author(s) and the source, provide a link to the Creative Commons licence, and indicate if changes were made. The images or other third party material in this article are included in the article's Creative Commons licence, unless indicated otherwise in a credit line to the material. If material is not included in the article's Creative Commons licence and your intended use is not permitted by statutory regulation or exceeds the permitted use, you will need to obtain permission directly from the copyright holder. To view a copy of this licence, visit <http://creativecommons.org/licenses/by/4.0/>.

## References

- Ajamzadeh MR et al (2018) The effect of micro parameters of PFC software on the model calibration. *Smart Struct Syst* 22(6):643–662. <https://doi.org/10.12989/sss.2018.22.6.643>
- Boley C, Forouzandeh Y, Wagner S, Pratter P (2019) Scherverhalten von acrylatischen Injektionskörpern. *geotechnik* 43(1):31–39. <https://doi.org/10.1002/gete.201900013>
- Chhun K-T, Lee S-H, Keo S-A, Yune C-Y (2019) Effect of acrylate-cement grout on the unconfined compressive strength of silty sand. *KSCE J Civ Eng* 23(6):2495–2502. <https://doi.org/10.1007/s12205-019-1968-z>
- Ciardi G, Vannucchi G, Madiari C (2021) Effects of colloidal silica grouting on geotechnical properties of liquefiable

- soils: a review. *Geotechnics* 2021(1):460–491. <https://doi.org/10.3390/geotechnics1020022>
- Da Silva LFM, Öchsner A, Adams R (2011) *Handbook of adhesion technology*. Springer, Berlin
- Forouzandeh Y, Boley C, Pratter P, Tintelnot G (2020) Numerische und experimentelle Untersuchung von Chancen und Risiken der Felsstabilisierung durch Injektion. HSSR, TU Graz
- Gu Y, Zhao J, Johnson JA (2020) Polymer networks: from plastics and gels to porous frameworks. *Angew Chem* 59(13):5022–5049. <https://doi.org/10.1002/anie.201902900>
- Habenicht G (2009) *Kleben*. Springer, Berlin
- Han J (2014) Recent research and development of ground column technologies. *Ice Ground Improvem* 168(GI4):246–264. <https://doi.org/10.1680/grim.13.00016>
- Hoek E (2007) Rock mass properties. In: *Practical rock engineering*. RocScience
- Holt RM et al (2005) Comparison between controlled laboratory experiments and discrete particle simulations of the mechanical behaviour of rock. *Int J Rock Mech Min Sci* 42:985–995
- Itasca Consulting Group Inc (2021) PFC–particle flow code in 2 and 3 dimensions, version 7.0, documentation set of version 7.00.132. Mineapolis
- Jose JP, Malhotra SK, Thomas S, Kuruvilla J, Goda K, Sreekala MS (2012) Advances in polymer composites: Macro- and microcomposites–state of the art, new challenges, and opportunities. In: *Polymer composites, Vol 1*, Wiley-VCH, Weinheim, pp 3-16
- Karol RH (2003) *Chemical grouting and soil stabilization*. CRC Press, Boca Raton
- Kutzner C (1991) *Injektionen im Baugrund*. Ferdinand Enke, Stuttgart
- Mezger TG (2018) *Applied rheology: with joe flow on rheology road*. Anton Paar, Graz
- Ozgurel HG, Vipulanandan C (2005) Effect of grain size and distribution on permeability and mechanical behavior of acrylamide grouted sand. *J Geotech Geoenviron Eng* 131(12):1457–1465. [https://doi.org/10.1061/\(ASCE\)1090-0241\(2005\)131:12\(1457\)](https://doi.org/10.1061/(ASCE)1090-0241(2005)131:12(1457))
- Persoff P, Apps J, Moridis G, Whang JM (1999) Effect of dilution and contaminants on sand grouted with colloidal silica. *J Geotech Geoenviron Eng* 125(6):461–469. [https://doi.org/10.1061/\(ASCE\)1090-0241\(1999\)125:6\(461\)](https://doi.org/10.1061/(ASCE)1090-0241(1999)125:6(461))
- Potyondy D (2018) Calibration of the flat-jointed material. PowerPoint Slide Set (April 13, 2018)
- Potyondy DO, Cundall PA (2004) A bonded-particle model for rock. *Int J Rock Mech Min Sci* 41(8):1329–1364. <https://doi.org/10.1016/j.ijrmms.2004.09.011>
- Spagnoli G (2018) A review of soil improvement with non-conventional grouts. *Int J Geotech Eng* 15(3):273–287. <https://doi.org/10.1080/19386362.2018.1484603>
- Webber MJ, Tibbitt MW (2022) Dynamic and reconfigurable materials from reversible network interactions. *Nat Rev Mater*. <https://doi.org/10.1038/s41578-021-00412-x>
- Zhao Y, Konietzky H, Herbst M (2021) Damage evolution of coal with inclusions under triaxial compression. *Rock Mech Rock Eng* 54:5319–5336. <https://doi.org/10.1007/s00603-021-02436-9>

**Publisher's Note** Springer Nature remains neutral with regard to jurisdictional claims in published maps and institutional affiliations.